# Stereo Particle Image Velocimetry Measurements of Transition Downstream of a Forward-Facing Step in a Swept-Wing Boundary Layer

Jenna L. Eppink*

*NASA Langley Research Center, Hampton, VA 23681*

**Stereo particle image velocimetry measurements were performed downstream of a forward-facing step in a stationary-crossflow dominated flow. Three different step heights were studied with the same leading-edge roughness configuration to determine the effect of the step on the evolution of the stationary-crossflow. Above the critical step height, which is approximately 68% of the boundary-layer thickness at the step, the step caused a significant increase in the growth of the stationary crossflow. For the largest step height studied (68%), premature transition occurred shortly downstream of the step. The stationary crossflow amplitude only reached approximately 7% of $U_e$ in this case, which suggests that transition does not occur via the high-frequency secondary instabilities typically associated with stationary crossflow transition. The next largest step of 60% $\delta$ still caused a significant impact on the growth of the stationary crossflow downstream of the step, but the amplitude eventually returned to that of the baseline case, and the transition front remained the same. The smallest step height (56%) only caused a small increase in the stationary crossflow amplitude and no change in the transition front. A final case was studied in which the roughness on the leading edge of the model was enhanced for the lowest step height case to determine the impact of the stationary crossflow amplitude on transition. The stationary crossflow amplitude was increased by approximately four times, which resulted in premature transition for this step height. However, some notable differences were observed in the behavior of the stationary crossflow mode, which indicate that the interaction mechanism which results in the increased growth of the stationary crossflow downstream of the step may be different in this case compared to the larger step heights.**

## Nomenclature

| | |
|---|---|
| $c$ | chord length |
| $C_p$ | Pressure coefficient, $C_p = \frac{p-p_\infty}{\frac{1}{2}\rho U_\infty^2}$ |
| $f$ | frequency |
| $h$ | step height |
| $Re'$ | Unit Reynolds number |
| $Tu$ | turbulence intensity |
| $U', V', W'$ | steady disturbance velocity |
| $u', v', w'$ | fluctuating components of velocity |
| $U'_{rms}$, $V'_{rms}$,'$W'_{rms}$ | spanwise root mean square of steady disturbance velocity |
| $U, V, W$ | velocity components in the $x$, $y$, and $z'$ directions |
| $U_e$ | boundary layer edge velocity |
| $U_\infty$ | freestream velocity |
| $x$ | streamwise direction |
| $x_h$ | streamwise location of step |

*Research Aerospace Engineer, Flow Physics and Control Branch, M.S. 170, AIAA Member

| | |
|---|---|
| $x_{sh}$ | number of step heights downstream of step |
| $y$ | wall-normal direction |
| $z$ | spanwise direction (parallel to the leading edge) |
| $z'$ | direction normal to side-wall |

*Symbols*

| | |
|---|---|
| $\delta$ | boundary layer thickness |
| $\lambda_z$ | spanwise wavelength |

# I. Introduction

LAMINAR flow control remains a promising technique for improving the fuel efficiency of aircraft in the near future. In theory and in the laboratory, laminar flow control (LFC) techniques can work quite well. However, real-world applications result in additional difficulties that can be detrimental if not well-managed. One such difficulty is the disruption of laminar flow that can occur if small protuberances or surface imperfections are present on the wing surface. These imperfections can result from insect residue, rivets, bolts, steps, gaps, paint, and other sources. In order for LFC to be effective in an operational environment, it is crucial that we gain a better understanding of how surface irregularities affect transition. This is important so that more reasonable manufacturing tolerances can be specified.

One approach to predicting the effect of 2D excrescences on transition is the use of a semiempirical method to estimate an expected increment in N-factors ($\Delta N$) across steps and gaps.[1–5] These studies have mostly focused on 2D (unswept) geometries,[1,5,6] but the effect of 2D steps on swept-wing transition has begun to gain more interest recently. This work was initially limited to observing the behavior of the transition front as the step height was increased,[3,7] but more recently, researchers have begun to study the flow in more detail.[8–12] These types of studies are important due to the complexity of the transition process over excrescences. The understanding is that the modified boundary layer due to the step will interact with the instabilities in the flow, causing either an increase in growth or a decrease (or no change). How these interactions affect the instabilities, what (if any) new types of instabilities are introduced by the step, and how these new instabilities interact to lead to transition are all problems that need to be addressed in order to better understand and predict transition in these cases.

Balakumar et al.[10] performed a computational study on the effect of backward- and forward-facing steps on a supersonic swept wing. They found that the backward-facing step has a small effect on the stationary crossflow mode, but the forward-facing step did not cause any noticeable change in amplitude. However, the authors believe that the step heights may have been too low to see any effect, since the forward-facing steps studied were the same height as the backward-facing steps. Typically, the critical forward-facing step height will be higher than the critical backward-facing step height.

Duncan et al.[9] performed hotwire measurements downstream of forward- and backward-facing steps to determine the effect of the steps on stationary crossflow instabilities. They found that the steps caused an increase in N-factor for the stationary crossflow. The forward-facing step (FFS) caused a larger growth of the stationary crossflow than the backward-facing step (BFS), but the critical backward-facing steps were lower than for the forward-facing steps, indicating that stationary crossflow was not the main transition mechanism for the BFS cases. Tufts et al.[11] performed computations to study the interaction between stationary crossflow instabilities and a two-dimensional step excrescence. The forward-facing step, above a critical height, was found to substantially increase the growth of the stationary crossflow mode. Additionally, they suggest a simple approach that may be used to predict the critical step height. They show that the likely mechanism that causes the enhanced growth of the stationary crossflow is a constructive interaction between the incoming stationary crossflow vortex and the helical flow region downstream of the step. When the center of the incoming stationary crossflow vortex is above the step, the stationary crossflow vortex and helical flow regions will interact constructively. Thus, if one can predict the height of the center of the incoming crossflow vortex, they state that this may be a good prediction of the critical step height.

The current work utilizes the experiment setup by Eppink et al.[12] to study forward-facing step configurations. Stereo particle image velocimetry (SPIV) measurements were performed for forward-facing steps of varying heights in order to investigate the effect of the steps on the stationary crossflow instabilities and to test the approach proposed by Tufts et al. for predicting the critical step height.

## II. Experimental Setup

The experiment was performed in the 2-Foot by 3-Foot Low Speed Boundary-Layer Channel at NASA Langley Research Center. The tunnel is a closed circuit facility with a 0.61-m high by 0.91-m wide by 6.1-m long test section. The tunnel can reach speeds up to 45 m/s ($Re' = 2.87$ x $10^6$/m) in the test section. Freestream turbulence intensity levels, $Tu = \frac{1}{U_\infty}\sqrt{\frac{1}{3}(u'^2 + v'^2 + w'^2)}$, were measured using a crosswire in an empty test section to be less than 0.06% for the entire speed range of the tunnel, and less than 0.05% for the test speed of 26.5 m/s. This value represents the total energy across the spectrum, high-pass filtered at 0.25 Hz. Thus, this tunnel can be considered a low-disturbance facility for purposes of conducting transition experiments.[13]

The 0.0127-m thick flat plate model consists of a 0.41-m long leading edge piece, swept at 30°, and a larger downstream piece (see Fig. 1). The model is 0.91 m wide (thus, spanning the width of the test section) and 2.54 m long on the longest edge. The length of the longest edge is taken to be the chord length, $c$, throughout this study. The downstream or leading edge pieces can be adjusted relative to each other using precision shims to create either forward-facing or backward-facing 2D steps of different heights, parallel with the leading edge. The leading edge piece was polished to a surface finish of 0.2 $\mu$m, and the larger downstream plate had a surface finish of 0.4 $\mu$m. A leading-edge contour was designed for the bottom side of the plate in order to make the suction-peak less severe, and therefore, avoid separation, which could potentially cause unsteadiness in the attachment line.

A 3D pressure body along the ceiling was designed to induce a streamwise pressure gradient, which, along with the sweep, causes stationary crossflow growth. A second purpose of the ceiling liner was to simulate infinite swept-wing flow within a mid-span measurement region of width 0.3 meters. This was achieved by designing the liner such that the $C_p$ contours were parallel with the leading edge within the measurement region. The ceiling liner was fabricated out of a hard foam using a computer-controlled milling machine.

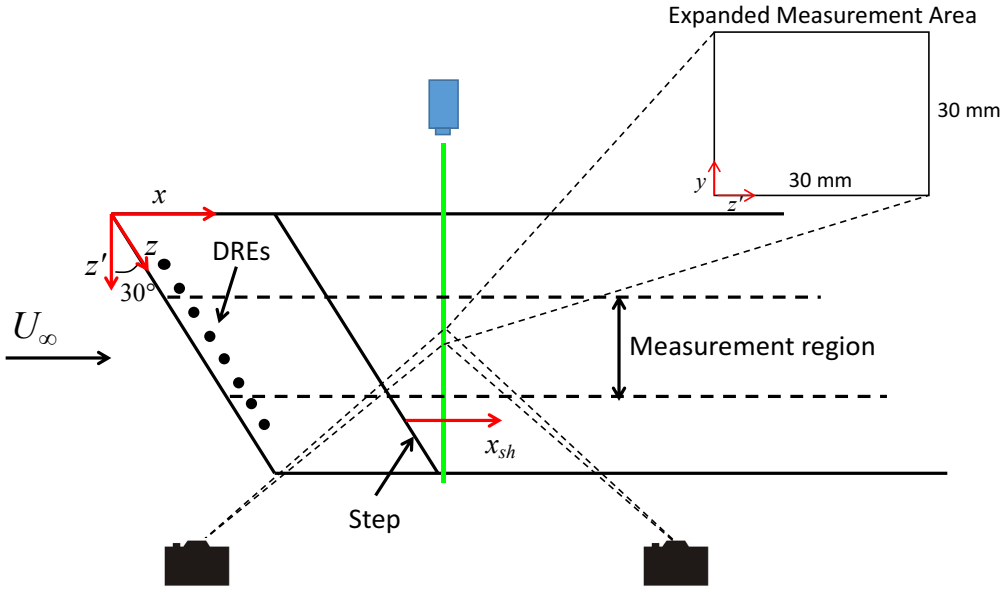


**Figure 1: Top view of PIV setup.**

All measurements were performed at a freestream velocity of 26.5 m/s ($Re' = 1.69$ x $10^6$/m). The current experiment utilized a leading-edge roughness configuration consisting of discrete roughness elements (DREs) with a diameter of 4.4 mm. The DREs were applied with a spanwise spacing, $\lambda_z$, of 11 mm and were approximately 20 $\mu$m thick. The spacing of the DREs (11 mm) corresponds to the most amplified stationary crossflow wavelength calculated for the baseline case (i.e., with no step). For more details of the experiment setup, refer to Eppink.[14]

A 200 mJ double-pulsed Nd:YAG laser was used to provide the laser sheet for the SPIV measurements. The laser sheet was set up as a y-z' plane, perpendicular to the freestream flow direction (see Fig. 1). Ideally, the measurements would be performed in a plane parallel with the step, and thus the laser sheet would need to be parallel with the step. It was not possible to get the light sheet parallel with the step due to optical limitations with the current setup, but modifications are planned to allow this improvement for future measurements. Two 2 megapixel cameras were placed on the outboard side of the test section at a 45° angle to the laser sheet. To achieve the desired field of view and resolution, 300 mm lenses were utilized, resulting in a measurement area of approximately 30 mm x 30 mm. This area allows acquisition of three wavelengths of the stationary crossflow instability in a single frame, while still acquiring approximately 25 points (using 75% overlap) inside the boundary layer. The cameras and laser were all mounted on the same traversing system, which allowed measurements at multiple locations with relative ease. The seeding, which was generated by an oil-based fog machine, was introduced downstream of the test section.

The stationary crossflow developed very quickly downstream of the step, and therefore, it was necessary to perform the data analysis on planes that were parallel with the step. With the current setup, only planes perpendicular to the flow were acquired. In order to acquire planes parallel with the step, multiple planes of data were acquired with 0.5 mm spacing in the streamwise direction. Thus, a volume of data could be constructed from the mean data, and planes parallel with the step could be extracted with 1-mm spanwise resolution (see Fig. 2). To save time, 100 image pairs were acquired for these measurements, since this was found to be sufficient to acquire mean values. The PIV results were found to compare well with the previously acquired hotwire results for the backward-facing step cases that were studied. These comparisons can be found in Eppink and Yao.[15]

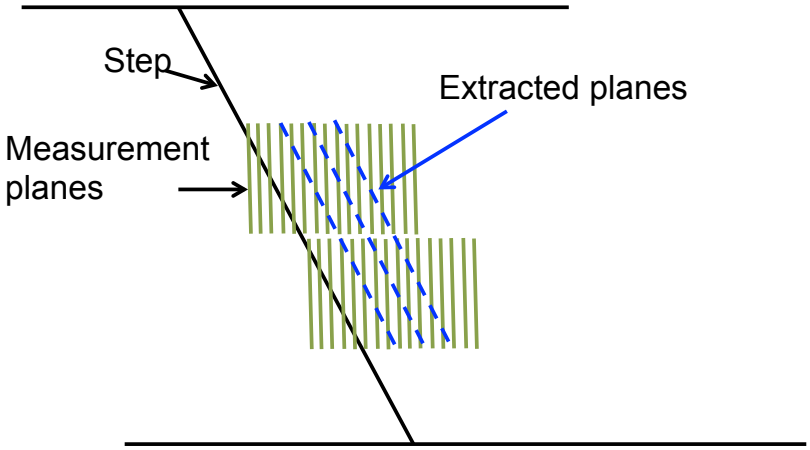


**Figure 2: Sketch of data collection procedure.**

## III. Results

### A. Effect of Step Height on Stationary Crossflow

SPIV measurements were performed for three different step heights of 1.4, 1.5, and 1.7 mm, and for the baseline (no-step) case. The step heights correspond to 56, 60, and 68% of the boundary layer thickness ($\delta$) at the step, respectively. For these cases, one layer (approximately 20 $\mu$m thick) of the 11-mm spaced DREs was applied approximately 50 mm downstream of the leading edge. Approximate transition locations for the four cases, obtained from naphthalene flow-visualization, are plotted in Fig. 3. No effect is seen on the transition front for the 1.4 and 1.5 mm step height cases, but at 1.7 mm, the transition front moves almost all the way forward to the step.

The effect of the step on the mean flow is shown in Fig. 4 as contour plots of the $U$ and $W$ velocity profiles versus $x_{sh}$. The profiles plotted here were averaged across each extracted $y$-$z$ plane to obtain the average profile at each streamwise location. While it is expected that there is a recirculating region close to the step, no recirculating region is readily apparent from the data that were acquired for any of the step heights. Tufts et al.[11] report that this top recirculating bubble is typically fairly long (approximately 2 to

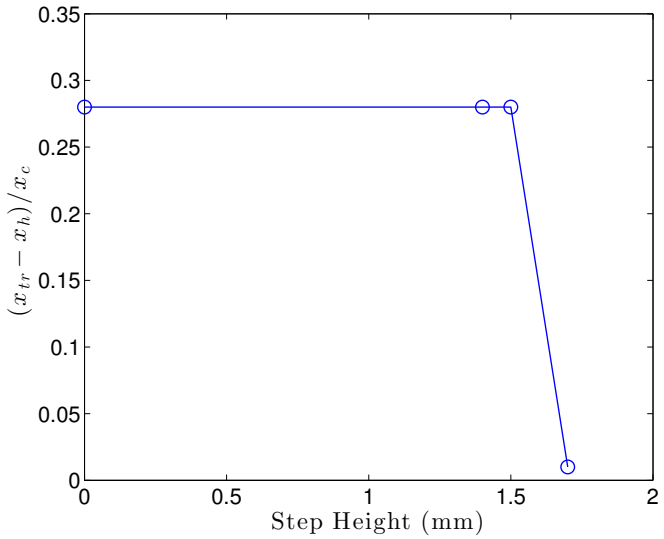


**Figure 3: Approximate transition location vs. step height.**

5 times the step height), but also quite thin, with the height only a small fraction of the step height. Thus, the height of the recirculating region may be so small that we were not able to measure close enough to the model surface to pick it up. In many cases, scattering off of dust particles on the surface of the model or off of the model made it difficult to acquire valid data very close to the wall. The recirculating region may also have been too weak for the technique to pick up any reversed flow.

As expected, the step causes a short region of adverse pressure gradient downstream of the step, which is apparent from the $U$ contours on the left. The effect of the step on the mean flow contours becomes more and more pronounced as the step height is increased. For the largest step height case of 1.7 mm, the boundary layer begins to transition to turbulence. This can be observed from the shape of the mean boundary layer profiles, which begin to broaden starting at approximately 10 step heights downstream of the step.

In all three cases, the boundary layers just downstream of the step include a region close to the wall ($y \approx 0.5$ mm) in which the $W$ velocity is strongly negative. The amplitude of this negative component becomes smaller as the flow progresses downstream of the step, but a negative component still remains for the smallest step height case. This is consistent with the boundary layers in the baseline case, which contains a small region near the wall where the $W$ velocity is slightly negative. The amplitude of the strong negative $W$ velocity near the wall appears to weaken as the step height increases. In fact, for the two larger step height cases, below this negative $W$ location, the $W$ velocity becomes positive near the wall. The positive component is stronger for the larger step height, and remains downstream as the flow becomes turbulent.

The steady $U$-perturbation profiles are plotted in Fig. 5 for each of the three step heights examined, both as individual profiles at selected locations (left) and as contour plots of $U'_{rms}/U_e$ vs $x_{sh}$ (right). The plots on the left also include a plot of the $U$-perturbation profile near the step location for the baseline case. Note that the x-scales are different in the plots on the left, and the color scales are different in the contour plots on the right. The profiles downstream of the 1.4 mm step do not appear vastly different from the baseline profile, both in terms of shape and amplitude (Fig. 5a). Despite the fact that the transition front did not move forward when the step height was raised to 1.5 mm, this step clearly affects the amplitude and shape of the stationary crossflow mode (Figs. 5c and 5d). The $U$-perturbation profiles close to the step ($x_{sh} \approx 1$ to 14) are double-peaked, with the larger amplitude peak occurring near the wall. The outer peak location is similar to the peak location of the baseline profile ($y \approx 1.2$ mm). Farther downstream the two peaks merge into one, and the maximum amplitude first decreases for a short length, then increases. The 1.7 mm step results (Figs. 5e and 5f) show a similar double-peaked behavior near the step, though the peak close to the wall is larger in amplitude (i.e., $x_{sh}$=6.8). Again, the two peaks merge into one as the amplitude initially decreases, then increases downstream. The observed behavior of the $U$-perturbation profiles agrees qualitatively with the results obtained computationally by Tufts et al.[11] for critical step heights.

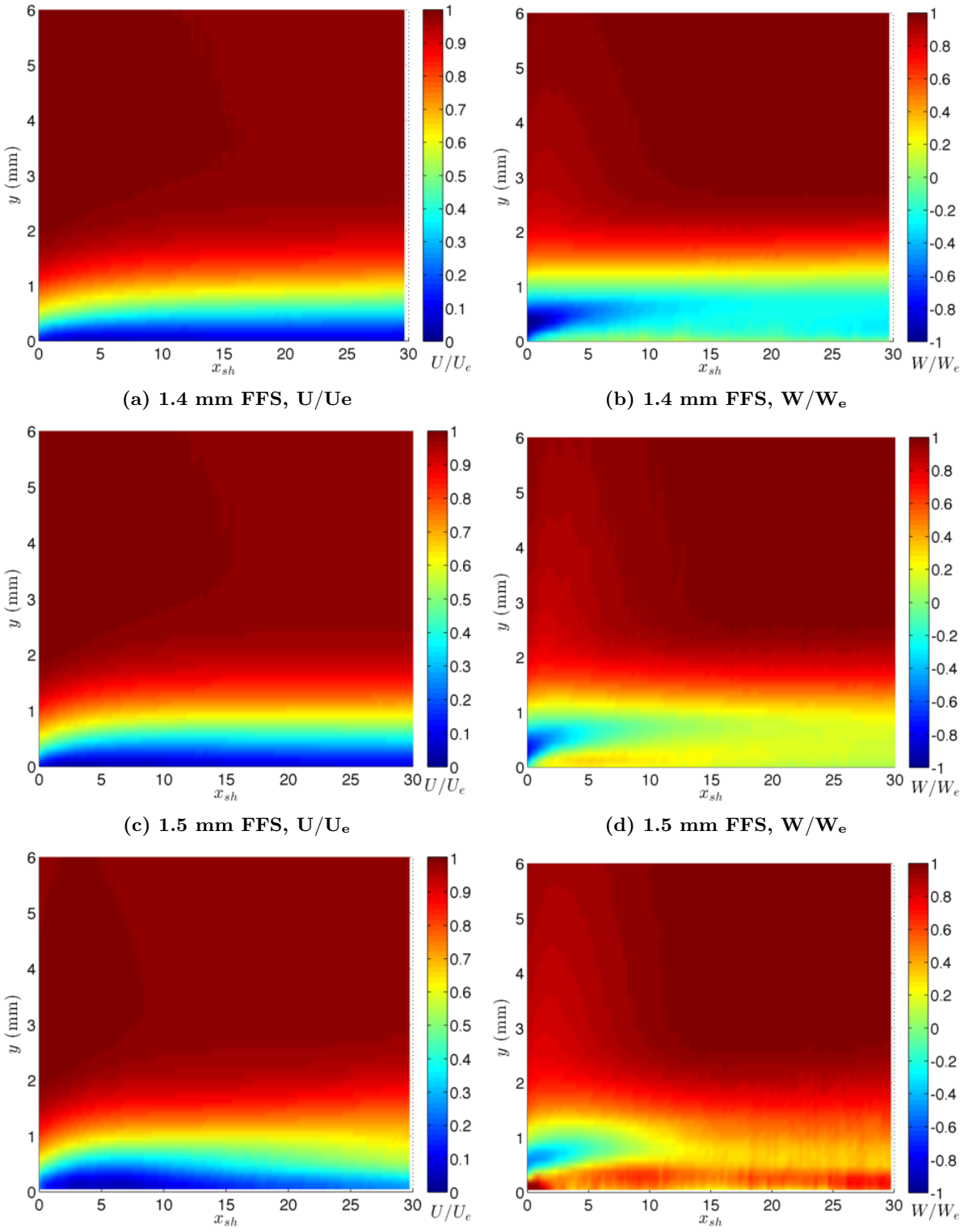


**(a) 1.4 mm FFS, U/Ue** **(b) 1.4 mm FFS, W/W$_e$**

**(c) 1.5 mm FFS, U/U$_e$** **(d) 1.5 mm FFS, W/W$_e$**

**(e) 1.7mm FFS, U/U$_e$** **(f) 1.7 mm FFS, W/W$_e$**

**Figure 4: Spanwise-averaged U and W velocity profiles vs. $x_{sh}$, for different step heights.**

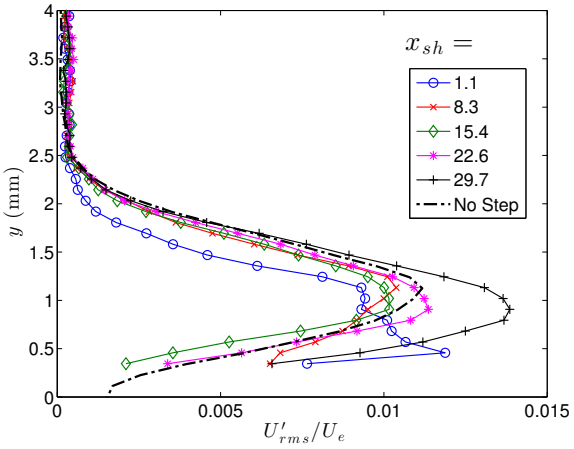


(a) 1.4 mm FFS

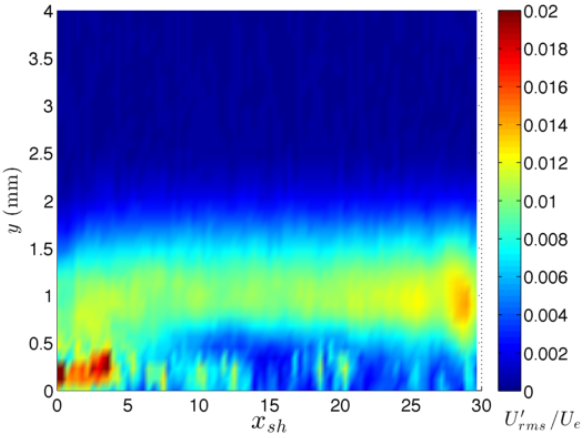


(b) 1.4 mm FFS

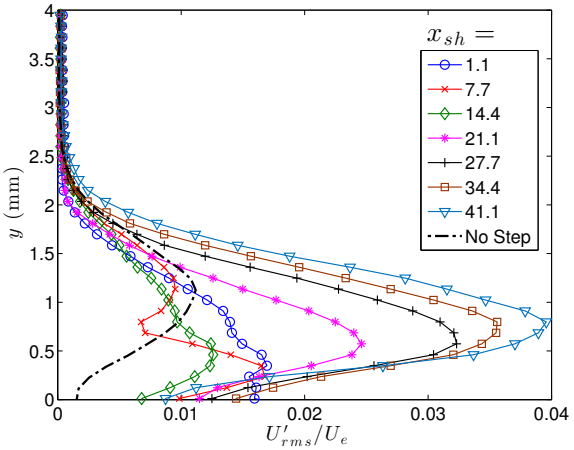


(c) 1.5 mm FFS

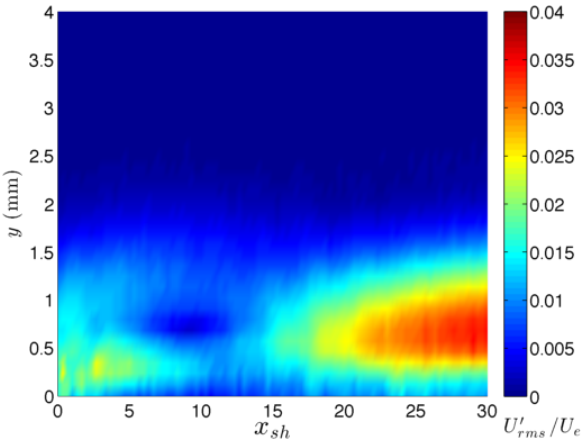


(d) 1.5 mm FFS

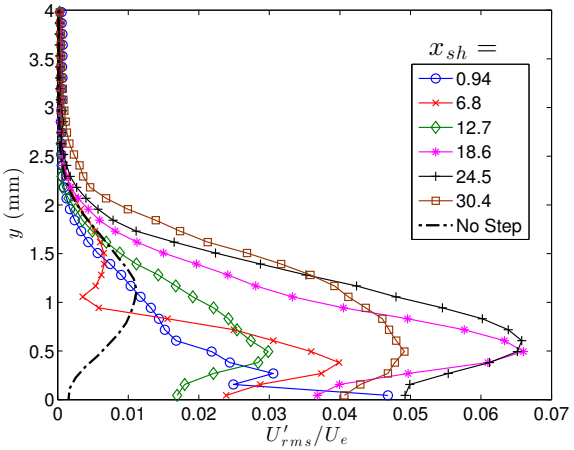


(e) 1.7mm FFS

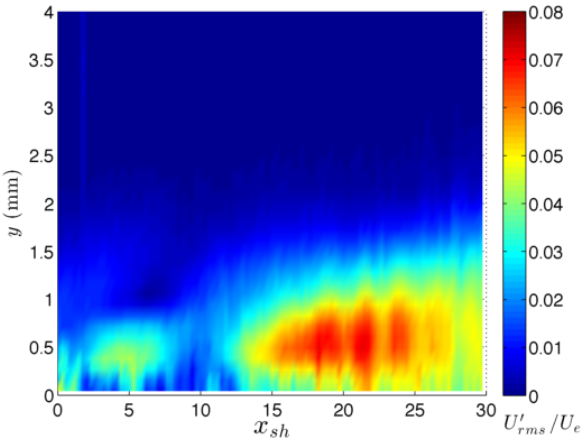


(f) 1.7 mm FFS

**Figure 5: U-perturbation profiles downstream of the step for all three step heights. Baseline profiles at $x_{sh}$=0 are also included.**

Figure 6 shows the maximum amplitude of each $U$-perturbation profile versus $x/c$ for each of the three step heights, as well as for the baseline case. The closely-spaced data points in this plot were obtained using the extracted-plane procedure described earlier. The more sparsely-spaced data points (i.e. the downstream points for the 1.4 mm and 1.5 mm FFS and baseline cases) were obtained from $x$-$z'$ planes (i.e. the "Measurement planes" in Fig. 2) rather than the extracted $x$-$z$ planes. This procedure was used so that more data could be quickly acquired and compared farther downstream of the step for the cases in which transition did not occur close to the step. Because the measurements are in different planes, there may be some difference in amplitude between the two methods, particularly near the step, since this is where the stationary crossflow changes the most rapidly moving downstream. This difference is evident for the 1.4 mm step case near the step. Just downstream of the 1.7 mm step, the amplitude of the stationary crossflow is approximately four times the amplitude in the baseline case. The amplitude quickly decays downstream, but then abruptly increases again, reaching an amplitude of approximately 7% before decaying. In this case, transition occurred just shortly (approximately 20 to 30 mm) downstream of the step, which corresponds to $x/c \approx 0.17$. The 1.5 mm step exhibits similar behavior, however, the amplitudes are about half that of the 1.7 mm step case, and transition does not occur prematurely. In this case, the maximum amplitude of 4% occurs at $x/c \approx 0.18$ before slowly decaying. Several stations were interrogated farther downstream to compare the amplitude to the baseline case. The amplitude begins to increase again farther downstream of the step, but it slowly begins to approach the amplitude of the baseline case. Since the stationary crossflow near the step did not reach a large enough amplitude to cause premature transition and then eventually returned to the amplitude in the baseline case, this explains why transition did not move upstream for the 1.5 mm step case, even though the stationary crossflow was clearly affected near the step. The 1.4 mm step does not appear to impact the stationary crossflow amplitude very near the step like the two larger step cases. However, starting at approximately $x/c = 0.17$, the amplitude increases relative to the baseline case, peaking at approximately $x/c = 0.18$, similar to the 1.5 mm step. The amplitude remains slightly larger than the stationary crossflow amplitude in the baseline case except for the most downstream measurement location.

These results show clearly that the forward-facing step has a significant impact on the stationary crossflow growth above a critical step height. However, for the 1.7 mm step case, which was the only case examined in this section that led to premature transition, the maximum amplitude that the stationary crossflow reached before breakdown occurred was approximately 7% of $U_e$. In a typical stationary crossflow breakdown scenario, the high-frequency secondary instabilities cause breakdown once the stationary crossflow causes a large distortion of the meanflow,[16–20] which typically requires amplitudes of at least 10 to 15% of the freestream velocity, as was seen in the baseline case for this experiment.[14] In the forward-facing step cases, the stationary crossflow amplitude is probably not large enough to cause breakdown via this high-frequency secondary instability, indicating that there may be some other instability present that is contributing to transition. The $u'_{rms}$ PIV results do show the presence of some unsteadiness in the flow, but due to the low number of samples acquired, the quality of these results is not sufficient to draw any conclusions, nor can we extract any frequency information. Further measurements using time-resolved PIV are planned to try to determine if any unsteady disturbances are destabilized due to the step.

The approach suggested by Tufts et al.[11] to predict the critical FFS height is to compute the linear-stability theory eigenfunctions for stationary crossflow and examine the Y-velocity ($V$) perturbation profile. The wall-normal location of the peak amplitude of the $V$-perturbation profiles should correspond approximately to the center of the crossflow vortex. They predict that when the step height is at or above the center of the crossflow vortex, the stationary crossflow and helical flow region that exists just downstream of the step will interact constructively to lead to the sudden amplification of the stationary crossflow instabilities downstream of the step. Figure 7 shows the computed and measured $V$-perturbation profiles near the step location for the 11-mm mode in the no-step case. The amplitude of the computed eigenfunction has been scaled to match the amplitude of the measured peak. There is excellent agreement between the measured and predicted mode shapes and peak locations, which occur at $y \approx 1.9$ mm. According to the approach that was just described, this means that the critical step height for the 11-mm stationary crossflow disturbance should be approximately 1.9 mm. The results discussed above show that the 1.7-mm step height is super-critical since it causes amplified growth of the stationary crossflow near the step, resulting in transition shortly downstream of the step. The 1.5-mm step height is considered near-critical, since it causes the stationary crossflow amplitude to increase initially, but eventually it relaxes back to the baseline case. While the 1.7-mm step height is somewhat smaller than the predicted 1.9-mm value, it is not much smaller. It is also expected

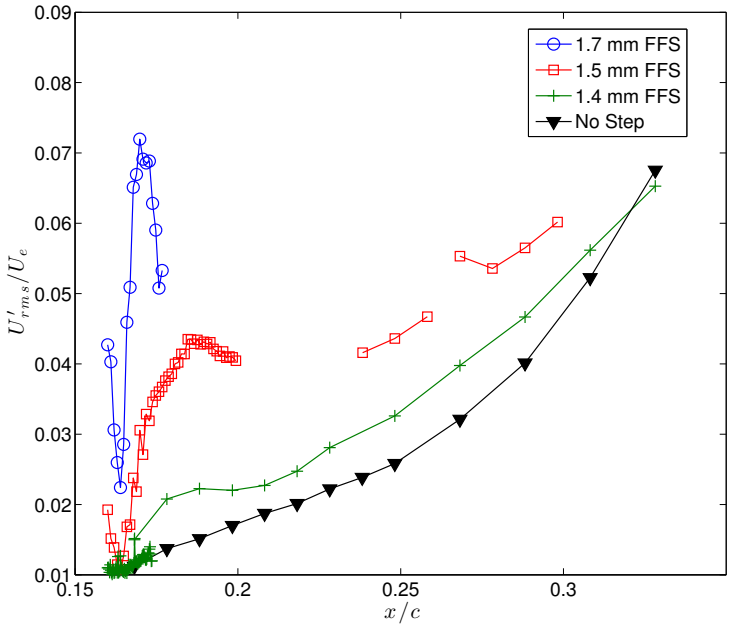


**Figure 6: Stationary crossflow amplitude vs. x/c for all three step heights and no-step case. The step is located at $x/c$=0.16.**

that one would need to take into account the height of the helical flow recirculating region downstream of the step when determining at which step height the stationary crossflow vortices and the helical flow region will interact constructively. Unfortunately, this region was not clearly captured by the PIV measurements, and there is no good rule of thumb for predicting the height of this region.[11]

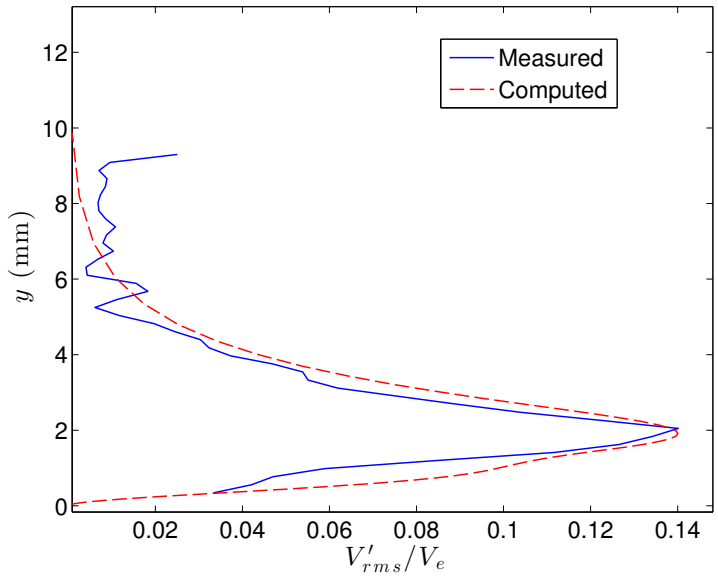


**Figure 7: Computed and measured $V$-perturbation profiles for baseline case.**

## B. Effect of Stationary Crossflow Amplitude

One additional case was investigated to determine whether a larger stationary crossflow amplitude at the step would lead to premature transition for a previously subcritical step height. For this case, the DREs were stacked to enhance the stationary crossflow amplitude at the step for the smallest subcritical step height, 1.4

mm. With two layers of DREs (approximately 40 $\mu$m tall), there was no noticeable effect on the transition front. Once three layers were stacked, the transition front was affected toward the outboard side of the measurement region, but not toward the inboard side. Thus, one additional layer was added (to make the DRE height approximately 80 $\mu$m), and the transition front moved upstream across the whole measurement region.

The spanwise-averaged mean flow results are plotted in Fig. 8 for the 1.4 mm step height with four layers of DREs applied. In this case, transition occurred by approximately $x/c = 0.19$, which is downstream of the region that was interrogated using PIV. The mean flow results look similar to the results for the 1.4 mm step height with a single layer of DREs (Fig. 4a).

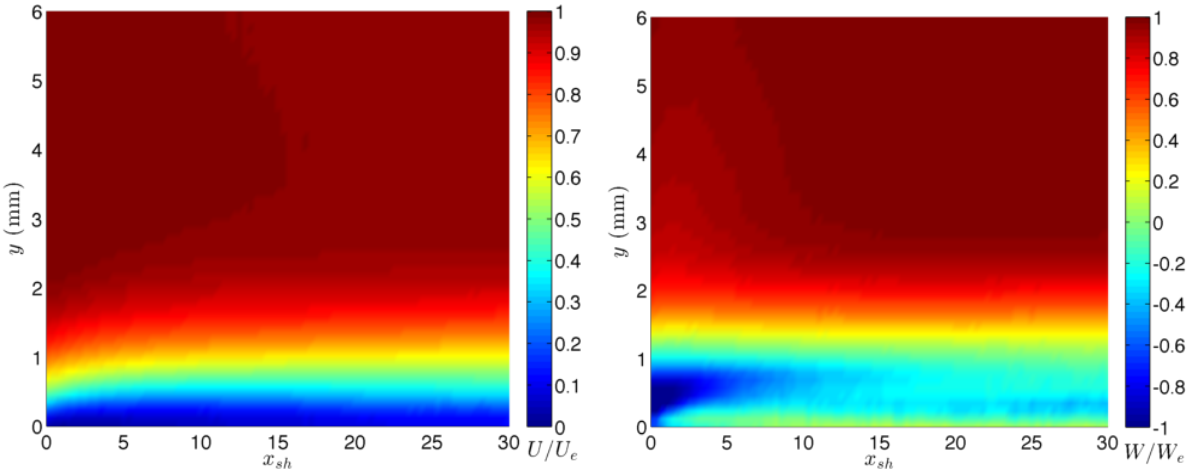


**(a) U/Ue** **(b) W/W$_e$**

**Figure 8: Spanwise averaged U and W velocity vs. $x_{sh}$ for 1.4 mm step height with 4 layers of DREs.**

The $U$-perturbation profiles for this case are plotted in Fig. 9. These are again plotted as individual profiles at selected locations (Fig. 9a), as well as a contour plot of amplitude versus $x_{sh}$ (Fig. 9b). Similar to the previous results for the 1.5 mm and 1.7 mm step cases (Fig. 5), the profiles near the step have two peaks ($x_{sh} \approx$1 to 8), though the peaks are not as distinct as in the 1.5 and 1.7 mm step cases. In this case, the peak closer to the wall decays shortly downstream of the step, whereas the upper peak does not undergo any decay before the amplitude increases and the shape starts to broaden. This is in contrast to the 1.5 and 1.7 mm step cases, in which the lower peak seems to dominate and feed into the larger amplitude peak downstream, while the upper peak decays (Figs. 5d and 5f)

Limited measurements were also acquired for the no-step case with 4 layers of DREs. These results are plotted along with all of the previous cases in Fig. 10, which shows the amplitude growth of the $U$-perturbation profiles. Note that the initial amplitude in this case is approximately 4 times larger than when a single-layer of DREs is applied. Comparing the amplitude growth of the 1.4 mm step case with 4 layers of DREs to the no-step case with the same leading edge roughness configuration, the step causes increased growth of the stationary crossflow mode very close to the step. The amplitude just downstream of the step is very similar to the 1.7 mm case, but the growth rate is slightly lower. The maximum amplitude for the 1.4 mm step case with 4 layers of DREs does undergo a short region of decay slightly downstream of the step, similar to the 1.5 and 1.7 mm step cases, but it does not decay as much as the 1.7 mm step case.

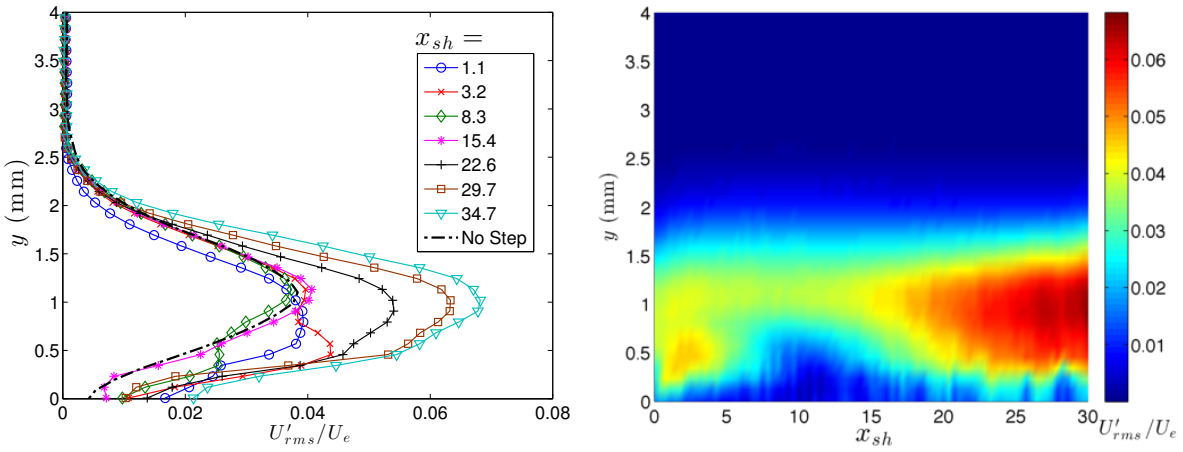


**(a) $U$ perturbation profiles** **(b) $U$ perturbation vs. $x_{sh}$**

**Figure 9: U perturbation profiles downstream of the step for the 1.4 mm step height with 4 layers of DREs. The no-step profile at $x_{sh}$=0 is also included.**

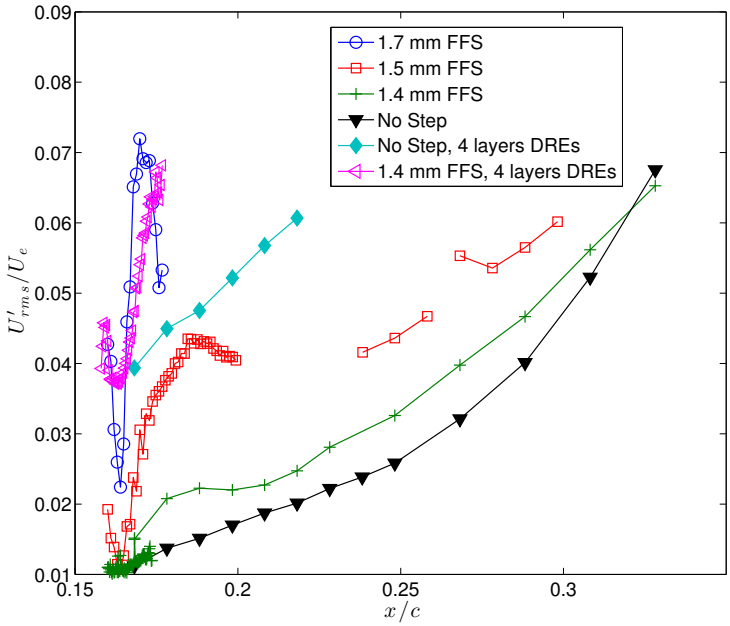


**Figure 10: Stationary crossflow amplitude vs. x/c for all three step heights and no-step case. The step is located at x/c=0.16.**

### C. Comparison of All Step Cases

Some interesting observations can be made by looking at the composite $x - z'$ and $y - z$ planes of data. Note that these were patched together from multiple planes of data (Fig. 2), which is the reason some of the contours do not appear smooth. The $x - z'$ planes of data at $y$=0.5 mm for the streamwise component of velocity are shown in Fig. 11 for all of the step cases that were studied. Measurements for the 1.5 mm step case extended farther downstream than for any of the other cases. Note that the color scales are different for each step case in order to show the various flow features more clearly. For the 1.5 mm step and the 1.7 mm step, the stationary crossflow undergoes a spatial shift just downstream of the step. This is evident in this figure because the strong high momentum and low momentum fluid regions shift outboard (right) by approximately half the wavelength of the stationary crossflow. This shift occurs approximately 10-20 mm

downstream of the step. In the 1.4 mm step case with 4 layers of DREs (Fig. 11d), the stationary crossflow also appears to shift spatially, but it appears that the vortices shift inboard (left) rather than outboard. The $x-z'$ plane plots of the $W$-velocity component reveal another interesting feature of the flow (Fig. 12). There is a smaller wavelength feature present that was not as visible in the $U$ component. This small wavelength feature is particularly evident in the 1.7 mm step case (Fig. 12c).

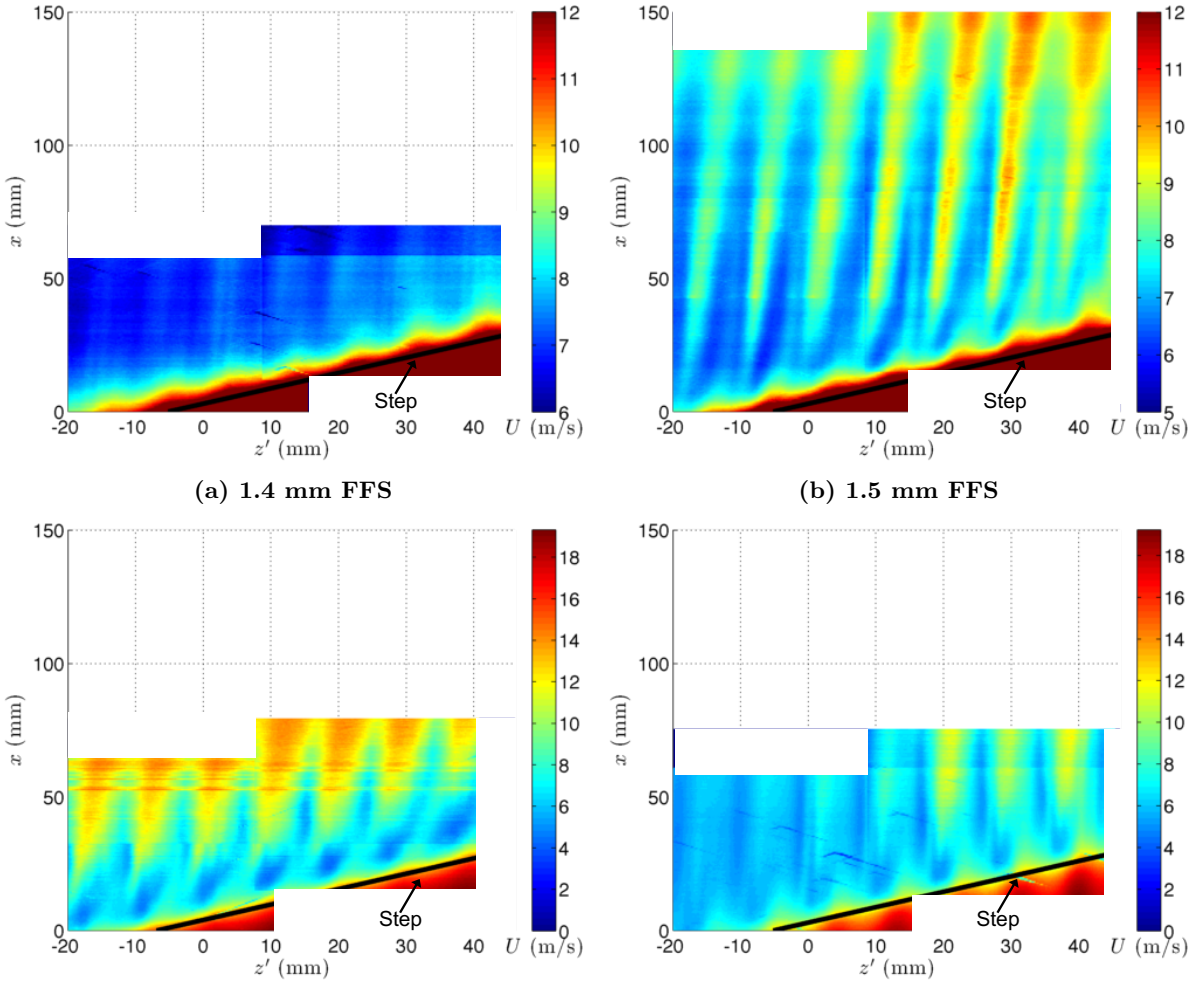


**(a) 1.4 mm FFS** **(b) 1.5 mm FFS**

**(c) 1.7 mm FFS** **(d) 1.4 mm FFS, 4 layers DREs**

**Figure 11: U velocity measurements in xz-plane at y=0.5 mm for all four step measurements.**

More observations about the behavior of the stationary crossflow downstream of the step can be made by examining the spanwise planes of the streamwise disturbance velocity ($U'/U_e$) close to the step. Two streamwise locations are shown for the 1.5 and 1.7 mm step heights in Fig. 13. Note that the color scales for the streamwise disturbance velocity plots are different for each step case. The double-peaked mode shape that was observed for these two step cases (Figs. 5c and 5e) is evident in these plots. In fact, it appears that the spatial phase of the outer peak is shifted from the inner peak by approximately half of the primary stationary crossflow wavelength.

From the spanwise plane plots, we can also observe the downstream phase shift that was described earlier in Figs. 11b and 11c. For instance, at $x_{sh} = 6$ for the 1.7 mm FFS case (Fig. 13c), a high speed flow region exists near the wall ($y \approx 0.5$ mm) at $z \approx 28$ mm. Downstream, at $x_{sh} = 16$ (Fig. 13d), we can see that this high speed region has now shifted to $z \approx 33$ mm. A similar shift occurs for the 1.5 mm step height (Fig. 13a and 13b).

There also seems to be a somewhat sudden shift in behavior moving downstream of $x_{sh} \approx 6$ for the 1.5 mm step case. The contours at $x_{sh}$=6 appear to be inclined to the left, but by $x_{sh} \approx 16$, the inclination

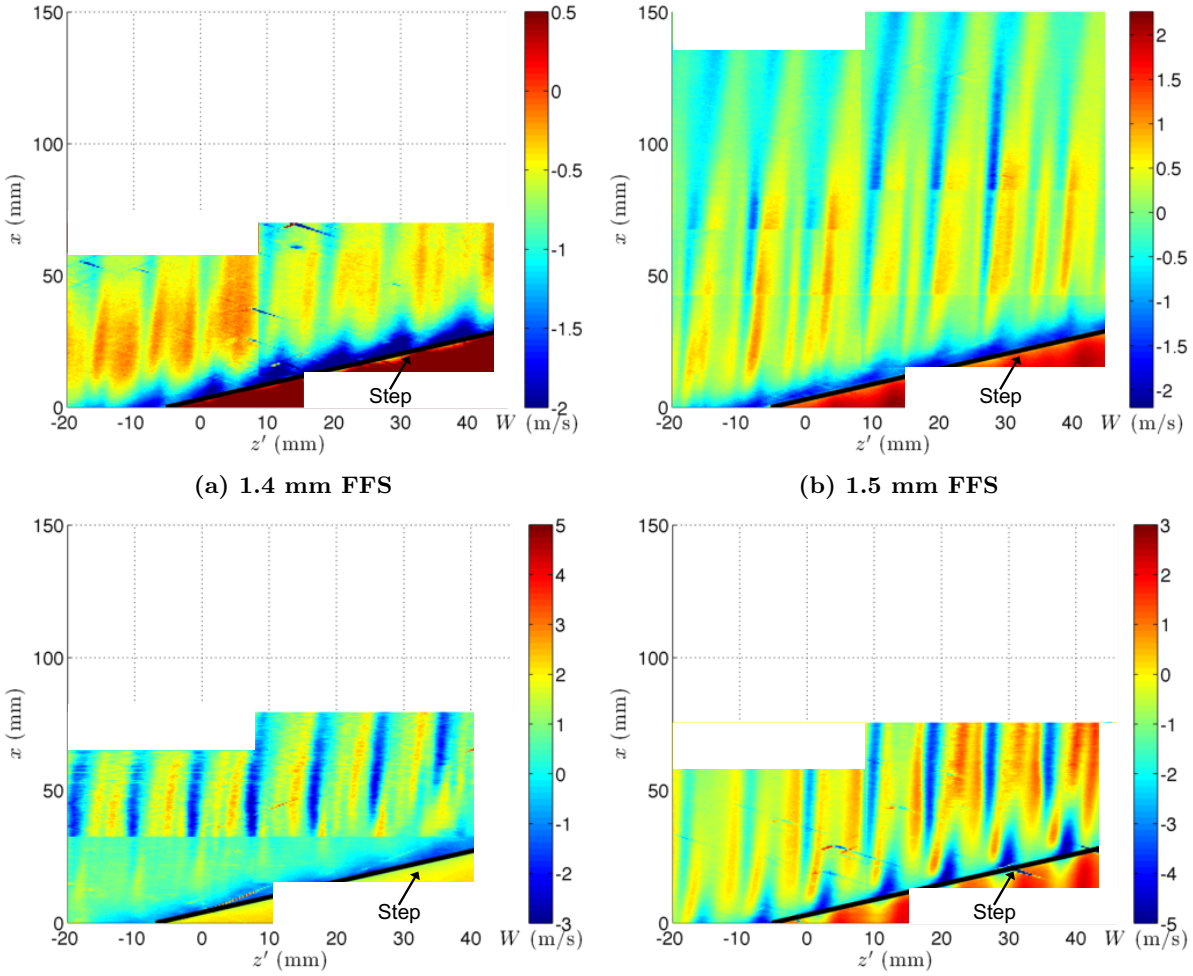


**(a) 1.4 mm FFS** **(b) 1.5 mm FFS**

**(c) 1.7 mm FFS** **(d) 1.4 mm FFS, 4 layers DREs**

**Figure 12: W velocity measurements in xz-plane at $y$=0.5 mm for all four step measurements.**

changes to the right. This behavior is also evident for the 1.7 mm step case at $x_{sh}$ ≈10 (see Fig. 14h). This shift may be due to a shearing effect because of the larger component of spanwise flow farther from the wall.

Similar spanwise plane results are shown for all of the cases examined in this study and for three streamwise locations in Fig. 14. Again, the color scales are different for each step case. The two 1.4 mm step cases show very similar behavior, except for the expected increase in amplitude for the case where four layers of DREs were applied. The 1.4 mm step case with 4 layers of DREs, though it also caused an increase in the growth of the stationary crossflow, does not exhibit the same behaviors that were described above for the 1.5 mm and 1.7 mm step cases. While there is some evidence of an inner and outer peak, there is not a clear phase shift evident between the two peaks. There is no obvious change in inclination of the contours as described for the 1.5 and 1.7 mm cases. There does appear to be a spanwise phase shift of the high and low momentum velocity regions moving from $x_{sh}$=6 to 16, but the shift is very small (approximately 2 mm), and the direction of the shift is to the left (inboard) rather than to the right. This was also evident from the $x - z'$ plane (Fig. 11d).

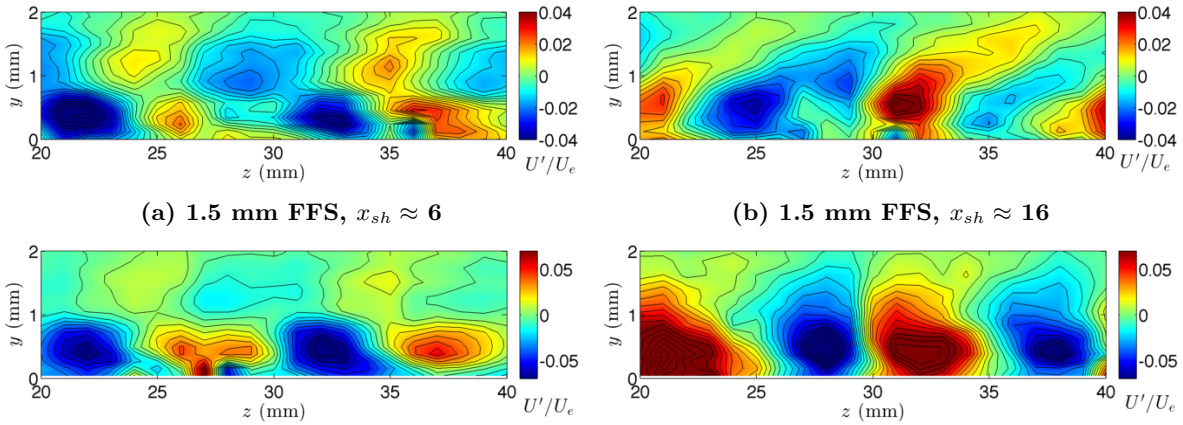


**(a) 1.5 mm FFS, $x_{sh} \approx 6$**

**(b) 1.5 mm FFS, $x_{sh} \approx 16$**

**(c) 1.7 mm FFS, $x_{sh} \approx 6$**

**(d) 1.7 mm FFS, $x_{sh} \approx 16$**

**Figure 13: Extracted spanwise planes of streamwise disturbance velocity ($U'/U_e$) for 1.5 and 1.7 mm steps at two streamwise locations.**

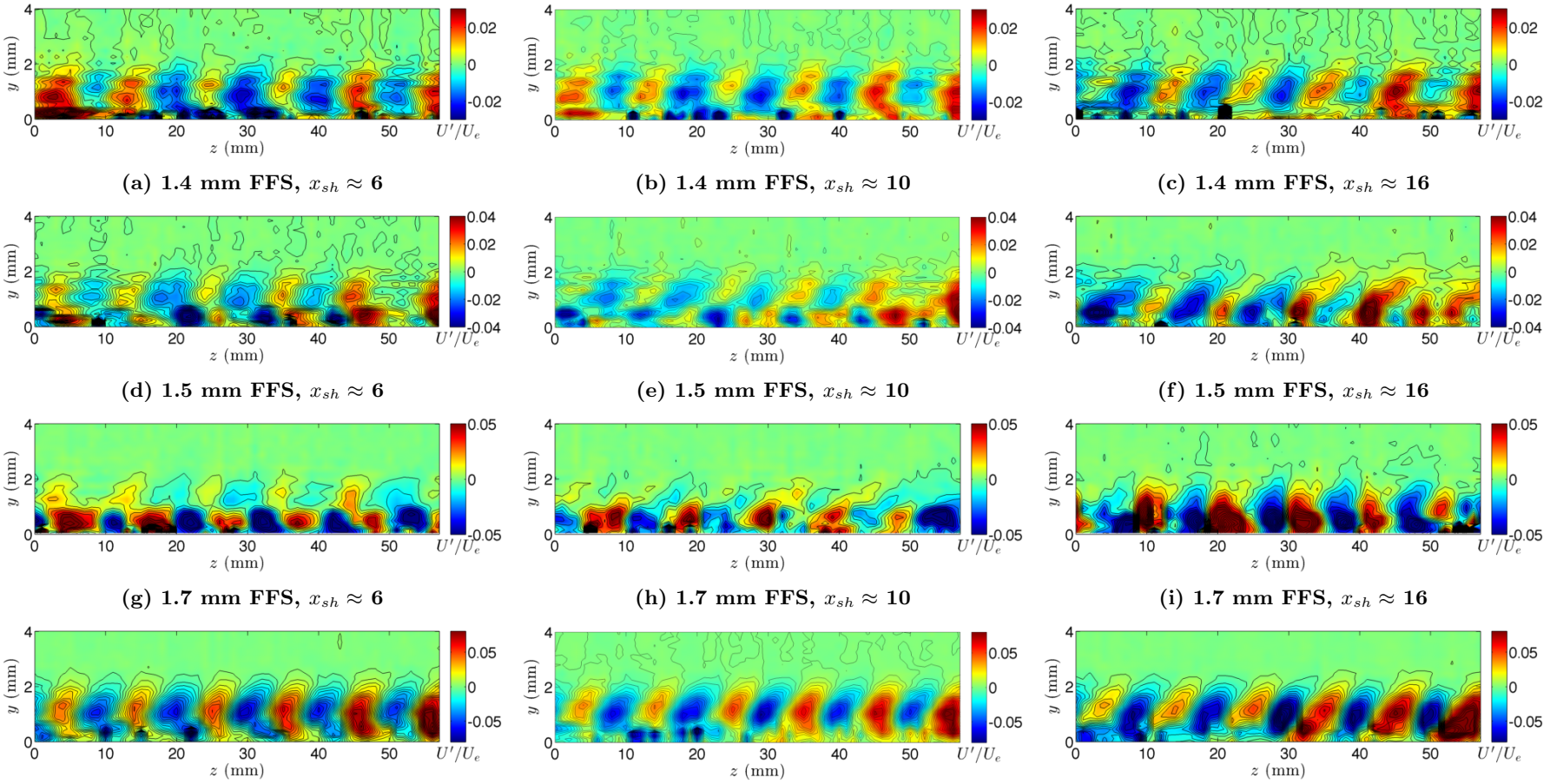


(a) 1.4 mm FFS, $x_{sh} \approx 6$ (b) 1.4 mm FFS, $x_{sh} \approx 10$ (c) 1.4 mm FFS, $x_{sh} \approx 16$

(d) 1.5 mm FFS, $x_{sh} \approx 6$ (e) 1.5 mm FFS, $x_{sh} \approx 10$ (f) 1.5 mm FFS, $x_{sh} \approx 16$

(g) 1.7 mm FFS, $x_{sh} \approx 6$ (h) 1.7 mm FFS, $x_{sh} \approx 10$ (i) 1.7 mm FFS, $x_{sh} \approx 16$

(j) 1.4 mm FFS, 4 layers of DREs, $x_{sh} \approx 6$ (k) 1.4 mm FFS, 4 layers of DREs, $x_{sh} \approx 10$ (l) 1.4 mm FFS, 4 layers of DREs, $x_{sh} \approx 16$

**Figure 14: Extracted spanwise planes of streamwise disturbance velocity ($U'/U_e$) for all step cases and three streamwise locations.**

## IV. Conclusions

The effect of forward-facing steps on stationary-crossflow growth was studied experimentally on a swept flat-plate model with an imposed pressure gradient. Measurements were performed using stereo particle image velocimetry. This technique not only allows acquisition of all three velocity components, but it also enables us to acquire full planes of data quickly (since it is not a point measurement like hotwire anemometry), which results in a rich and comprehensive data set.

Initially, the effect of step height on the stationary crossflow instability was examined by varying the step height for a single layer of DREs, in which the most amplified stationary crossflow mode was forced. The 1.7 mm step height was super-critical, causing a significant increase in the growth of the stationary crossflow downstream of the step, and resulting in premature transition shortly downstream of the step. The 1.5 mm step height also caused an increase in the growth of the stationary crossflow, but the amplitude eventually decayed and no change was seen in the transition front from the baseline case. The results agree qualitatively with the computational results obtained by Tufts et al.[11] Additionally, the predicted critical step height of 1.9 mm, which is obtained using the approach suggested by Tufts et al.[11] is close to the measured critical step height of 1.7 mm.

An additional configuration was tested for the smallest step height of 1.4 mm, in which the DREs on the leading edge of the model were stacked in order to increase the amplitude of the stationary crossflow instability. The objective of this test was to determine if increasing the amplitude of the stationary crossflow would affect the critical step height. Three layers of DREs were stacked before an effect was seen, but a fourth layer was added because the transition front became more uniform across the measurement region. With four layers of DREs applied, the amplitude of the stationary crossflow at the step was approximately four times that of the case with one layer of DREs applied. With a single layer of DREs applied, the 1.4 mm step case was subcritical. When four layers of DREs were applied, and thus the stationary crossflow amplitude increased by approximately four times, the step caused an increase in the growth of the stationary crossflow, and transition occurred shortly downstream of the step. There were several notable differences in the behavior of the stationary crossflow mode downstream of the step when comparing this case to the other near-critical and super-critical cases of 1.5 and 1.7 mm. This indicates that when the incoming stationary crossflow amplitude is large and the step is below the critical step height, the mechanism that causes the increased stationary crossflow growth may be different from the mechanism that occurs above the critical step height when the stationary crossflow amplitudes are lower.

In the two super-critical cases studied (1.7 mm step with a single layer of DREs, and 1.4 mm step with four layers of DREs), the stationary crossflow amplitudes reached values of approximately 7% $U_e$ before transition occurred. While this amplitude is significantly larger than the stationary crossflow amplitude in the no-step cases near the step, it is still probably too low to cause transition via the high-frequency secondary instabilities typically associated with stationary crossflow transition. Thus, there may be some other types of unsteady instabilities introduced by the step, or another type of secondary instability that ultimately leads to transition.

## V. Acknowledgments

This work was performed as part of the Revolutionary Computational Aerosciences discipline under the Transformational Tools and Technologies Project of the NASA Fundamental Aeronautics Program. The authors would like to thank Dr. Chung-Sheng Yao, Mark Fletcher, and Charles Debro for their support of the PIV setup and wind tunnel testing, and the members of the Flow Physics and Control Branch of NASA Langley Research Center for their support and many helpful discussions.

## References

[1]Crouch, J., Kosorygin, V., and Ng, L., "Modeling the Effects of Steps on Boundary-Layer Transition," *IUTAM Symposium on Laminar-Turbulent Transition*, Springer, 2006, pp. 37–44.

[2]Perraud, J., Séraudie, A., Reneaux, J., Arnal, D., and Tran, D., "Effect of 2D and 3D Imperfections on Laminar-Turbulent Transition," *CEAS Katnet Conf. on Key Aerodynamic Technologies*, 2005.

[3]Perraud, J. and Seraudie, A., "Effects of Steps and Gaps on 2D and 3D Transition," *European Congress on Comp. Methods in Applied Science and Eng., ECCOMAS*, 2000, pp. 11–14.

[4]Edelmann, C. and Rist, U., "Impact of Forward-Facing Steps on Laminar-Turbulent Transition in Transonic Flows

Without Pressure Gradient," AIAA Paper 2013-0080, 2013.

[5]Wörner, A., Rist, U., and Wagner, S., "Influence of Humps and Steps on the Stability Characteristics of a 2D Laminar Boundary Layer," AIAA Paper 2002-0139, 2002.

[6]Drake, A., Bender, A., Korntheuer, A., Westphal, R., McKeon, B., Gerashchenko, S., Rohe, W., and Dale, G., "Step Excrescence Effects for Manufacturing Tolerances on Laminar Flow Wings," AIAA Paper 2010-375, 2010.

[7]Duncan Jr, G., Crawford, B., and Saric, W., "Effects of Step Excrescences on Swept-Wing Transition," AIAA Paper 2013-2412, 2013.

[8]Saeed, T. I., Mughal, M. S., and Morrison, J., "The Interaction of a Swept-Wing Boundary Layer with Surface Excrescences," AIAA Paper 2016-2065, 2016.

[9]Duncan Jr, G. T., Crawford, B. K., Tufts, M. W., Saric, W. S., and Reed, H. L., "Effects of Step Excrescences on a Swept Wing in a Low-Disturbance Wind Tunnel," AIAA Paper 2014-0910, 2014.

[10]Balakumar, P., King, R. A., and Eppink, J. L., "Effects of Forward-and Backward-Facing Steps on the Crossflow Receptivity and Stability in Supersonic Boundary Layers," AIAA Paper 2014-2639, 2014.

[11]Tufts, M. W., Reed, H. L., Crawford, B. K., Duncan Jr, G. T., and Saric, W. S., "Computational Investigation of Step Excrescence Sensitivity in a Swept-Wing Boundary Layer," AIAA Paper 2015-2775, 2015.

[12]Eppink, J., Wlezien, R., King, R., and Choudhari, M., "The Interaction of Stationary Crossflow and a Backward-facing Step in Swept Boundary-Layer Transition," AIAA Paper 2015-0273, 2015.

[13]Saric, W. S. and Reshotko, E., "Review of Flow Quality Issues in Wind Tunnel Testing," AIAA Paper 1998-2613, 1998.

[14]Eppink, J., *The Interaction of Crossflow Instabilities and a Backward-Facing Step in Swept Boundary Layer Transition*, Ph.D. thesis, Tufts University, 2014.

[15]Eppink, J. and Yao, C.-S., "Stereo Particle Image Velocimetry Measurements of Transition Downstream of a Backward-Facing Step in a Swept-Wing Boundary Layer," *Submitted to AIAA Science and Technology Forum and Exposition*, Grapevine, TX, 2017.

[16]Kohama, Y., Saric, W., and Hoos, J., "A High-Frequency, Secondary Instability of Crossflow Vortices that Leads to Transition," *Proc. of the Royal Aero. Soc. Conf.*, 1991, pp. 1–12.

[17]Malik, M., Li, F., and Chang, C.-L., "Crossflow Disturbances in Three-Dimensional Boundary Layers:Nonlinear Development, Wave Interaction and Secondary Instability," *Journal of Fluid Mechanics*, Vol. 268, No. 1, 1994, pp. 1–36.

[18]Malik, M. R., Li, F., Choudhari, M. M., and Chang, C.-L., "Secondary Instability of Crossflow Vortices and Swept-Wing Boundary-Layer Transition," *Journal of Fluid Mechanics*, Vol. 399, 1999, pp. 85–115.

[19]White, E. and Saric, W., "Secondary Instability of Crossflow Vortices," *Journal of Fluid Mechanics*, Vol. 525, No. 1, 2005, pp. 275–308.

[20]Duan, L., Choudhari, M. M., and Li, F., "Direct Numerical Simulation of Transition in a Swept-Wing Boundary Layer," AIAA Paper 2013-2617, 2013.